Inorganic Chemistry
Article

Inorg. Chem. **2011**, *50*, 1973–1982 **1973**
DOI: 10.1021/ic102451n

New Second-Order NLO Materials Based on Polymeric Borate Clusters and GeO_4 Tetrahedra: A Combined Experimental and Theoretical Study

Jian-Han Zhang,[†,‡] Chun-Li Hu,[†] Xiang Xu,[†] Fang Kong,[†] and Jiang-Gao Mao*[,†]

[†]*State Key Laboratory of Structural Chemistry, Fujian Institute of Research on the Structure of Matter, Chinese Academy of Sciences, Fuzhou 350002, People's Republic of China, and* [‡]*Graduate School of the Chinese Academy of Sciences, Beijing, 100039, People's Republic of China*

Received December 7, 2010

Three novel rubidium borogermanates with three types of noncentrosymmetric structures, namely, $RbGeB_3O_7$, $Rb_2GeB_4O_9$, and $Rb_4Ge_3B_6O_{17}$, have been synthesized by high-temperature solid-state reactions in platinum crucibles. The structure of $RbGeB_3O_7$ features a three-dimensional (3D) anionic framework composed of cyclic B_3O_7 groups corner-sharing GeO_4 tetrahedra. The structure of $Rb_2GeB_4O_9$ shows a 3D anionic framework based on B_4O_9 clusters connected by GeO_4 tetrahedra via corner sharing. The structure of $Rb_4Ge_3B_6O_{17}$ is a novel 3D anionic framework composed of cyclic B_3O_8 groups, Ge_2O_7 dimers, and GeO_4 tetrahedra that are interconnected via corner sharing. Second harmonic generation (SHG) measurements indicate that $RbGeB_3O_7$, $Rb_2GeB_4O_9$, and $Rb_4Ge_3B_6O_{17}$ display moderate SHG responses that are approximately 1.3, 2.0, and 1.3 $\times$ KH_2PO_4 (KDP), respectively, which are slightly smaller than those from theoretical calculations (about 3.7, 2.8, and 2.4 $\times$ KDP, respectively).

Introduction

The search of new second-order nonlinear optical (NLO) material is of current interest and great importance owing to their applications in photonic technologies.[1] It is reported that inorganic compounds with asymmetric or polar coordination units are more likely to display noncentrosymmetric (NCS) structures and exhibit good second harmonic generation (SHG) properties. The presence of π-conjugated systems based on triangular BO_3 groups, d^0 transition metals with a distorted octahedral coordination geometry, and cations containing active lone pairs have been used to design new SHG materials. It has been demonstrated that the combination of above two types of building units can lead to a number of compounds with excellent SHG properties due to the "additive" effect of both types of polarization groups,[2−5] as exampled by $Cd_4BiO(BO_3)_3$,[3a] $Pb_2B_5O_9I$,[3b] $BaMo_2TeO_9$ and BaW_2TeO_9,[4a] $Se_2(B_2O_7)$,[5a] and $BaNbO(IO_3)_6$.[5b]

Though reports on metal borogermanates are still rather limited, they are able to form various NCS structures with possible SHG properties or zeolite-type open frameworks.[6−15] A series of organically templated layered or three-dimensional

*To whom correspondence should be addressed. E-mail: mjg@fjirsm.ac.cn. Fax: (+86)591-83714946.

(1) (a) Chen, C.; Liu, G. *Annu. Rev. Mater. Sci.* **1986**, *16*, 203. (b) Ok, K. M.; Halasyamani, P. S. *Chem. Soc. Rev.* **2006**, *35*, 710. (c) Wang, S. C.; Ye, N.; Li, W.; Zhao, D. *J. Am. Chem. Soc.* **2010**, *132*, 8779. (d) Pan, S.; Smit, J. P.; Watkins, B.; Marvel, M. R.; Stern, C. L.; Poeppelmier, K. R. *J. Am. Chem. Soc.* **2006**, *128*, 11631.

(2) (a) Chang, H. Y.; Kim, S. H.; Ok, K. M.; Halasyamani, P. S. *J. Am. Chem. Soc.* **2009**, *131*, 6865. (b) Yang, T.; Sun, J. L.; Yeon, J.; Halasyamani, P. S.; Huang, S. L.; Hemberger, J.; Gereenblatt, M. *Chem. Mater.* **2010**, *22*, 4814. (c) Chang, H. Y.; Kim, S. W.; Halasyamani, P. S. *Chem. Mater.* **2010**, *22*, 3241. (d) Chang, H. Y.; Kim, S. H.; Ok, K. M.; Halasyamani, P. S. *Chem. Mater.* **2009**, *21*, 1654.

(3) (a) Zhang, W. L.; Cheng, W. D.; Zhang, H.; Geng, L.; Lin, C. S.; He, C. Z. *J. Am. Chem. Soc.* **2010**, *132*, 1508. (b) Huang, Y. Z.; Wu, L. M.; Wu, X. T.; Li, L. H.; Chen, L.; Zhang, Y. F. *J. Am. Chem. Soc.* **2010**, *132*, 12788.

(4) (a) Ra, H. S.; Ok, K. M.; Halasyamani, P. S. *J. Am. Chem. Soc.* **2003**, *125*, 7764. (b) Kim, J. H.; Baek, J.; Halasyamani, P. S. *Chem. Mater.* **2007**, *19*, 5637. (c) Chi, E. O.; Ok, K. M.; Porter, Y.; Halasyamani, P. S. *Chem. Mater.* **2006**, *18*, 2070.

(5) (a) Kong, F.; Huang, S. P.; Sun, Z. M.; Mao, J. G.; Cheng, W. D. *J. Am. Chem. Soc.* **2006**, *128*, 7750. (b) Sun, C. F.; Hu, C. L.; Xu, X.; Ling, J. B.; Hu, T.; Kong, F.; Long, X. F.; Mao, J. G. *J. Am. Chem. Soc.* **2009**, *131*, 9486. (c) Yang, B. P.; Hu, C. L.; Xu, X.; Sun, C. F.; Zhang, J. H.; Mao, J. G. *Chem. Mater.* **2010**, *22*, 1545. (d) Jiang, H. L.; Huang, S. P.; Fan, Y.; Mao, J. G.; Cheng, W. D. *Chem.—Eur. J.* **2008**, *14*, 1972. (e) Hu, T.; Qin, L.; Kong, F.; Zhou, Y.; Mao, J. G. *Inorg. Chem.* **2009**, *48*, 2193.

(6) (a) Dadachov, M. S.; Sun, K.; Conradsson, T.; Zou, X. D. *Angew. Chem., Int. Ed.* **2000**, *39*, 3674. (b) Li, Y.; Zou, X. D. *Angew. Chem., Int. Ed.* **2005**, *44*, 2012. (c) Li, Y. F.; Zou, X. D. *Acta Crystallogr.* **2003**, *C59*, 471.

(7) (a) Pan, C. Y.; Liu, G. Z.; Zheng, S. T.; Yang, G. Y. *Chem.—Eur. J.* **2008**, *14*, 5057. (b) Wang, G. M.; Sun, Y. Q.; Yang, G. Y. *Cryst. Growth Des.* **2005**, *5*, 313. (c) Zhang, H. X.; Zhang, J.; Zheng, S. T.; Yang, G. Y. *Inorg. Chem.* **2005**, *44*, 1166. (d) Cao, G. J.; Fang, W. F.; Zheng, S. T.; Yang, G. Y. *Inorg. Chem. Commun.* **2010**, *13*, 1047.

(8) Zhang, J. H.; Li, P. X.; Mao, J. G. *Dalton Trans.* **2010**, *39*, 5301.

(9) Heymann, G.; Huppertz, H. *J. Solid State Chem.* **2006**, *179*, 370.

(10) Ilyukhin, A. B.; Dzhurinskii, B. F. *Russ. J. Inorg. Chem.* **1994**, *39*, 556.

(11) (a) Kaminskii, A. A.; Mill, B. V.; Belokoneva, E. L.; Butashin, A. V. *Inog. Mater.* **1990**, *26*, 934. (b) Belokoneva, E. L.; Mill, B. V.; Butashin, A. V.; Kaminskii, A. A. *Izv. Akad. Nauk SSSR, Neorg. Mater.* **1991**, *27*, 1700.

(12) (a) Lin, Z. E.; Zhang, J.; Yang, G. Y. *Inorg. Chem.* **2003**, *42*, 1797. (b) Zhang, H. X.; Zhang, J.; Zheng, S. T.; Wang, G. M.; Yang, G. Y. *Inorg. Chem.* **2004**, *43*, 6148.

Published on Web 01/13/2011

(3D) borogermanates has been reported by the Zou and Yang groups.[6,7] It is found that size, shape, and charge of the template cations may direct the formation of different open frameworks. Several types of lanthanide(III) borogermanates have also been reported,[8−11] among which $Ln_{14}(GeO_4)_2(BO_3)_6O_8$ and $LnGeBO_5$ ($P3_1$) are structurally acentric.[10,11a] Unfortunately, their SHG properties were not studied.

A series of alkali borogermanates has been synthesized, including $KBGe_2O_6$,[12a] $K_2[GeB_4O_9]\cdot 2H_2O$,[12b] $CsGeB_3O_7$, $K_2B_2Ge_3O_{10}$,[13] $LiBGeO_4$,[14] $K_4[B_8Ge_2O_{17}(OH)_2]$,[15a] and $NH_4(BGe_3O_8)$.[15b] The first five compounds are structurally acentric. More interesting, $K_2GeB_4O_9\cdot 2H_2O$ and $CsGeB_3O_7$ exhibit moderate SHG responses that are 2.0 and 1.5 × KH_2PO_4 (KDP), respectively.[12b,13] So far, no compounds in the Rb−Ge−B−O system have been reported. We suggest that the different ionic size of rubidium(I) from other alkali cations, such as cesium(I) and potassium(I), may lead to materials with different open frameworks. Furthermore, it is assumed that the different B/Ge ratios may lead to different boron−oxygen clusters and their different connectivity fashions with the GeO_4 units. No theoretical investigation on these new types of NLO materials has been performed. Our systematic investigations of new materials in the Rb−B−Ge−O system led to three novel rubidium borogermanates with noncentrosymmetric structures, namely, $RbGeB_3O_7$, $Rb_2GeB_4O_9$, and $Rb_4Ge_3B_6O_{17}$. They exhibit SHG responses of about 1.3, 2.0, and 1.3 × KDP, respectively. Herein, we report their syntheses, crystal structures, and electronic and optical properties.

Experimental Section

Materials and Methods. H_3BO_3 (Shanghai Reagent Factory, 99.9%), GeO_2 (Shanghai Reagent Factory, 99.99%), Rb_2CO_3 (Alfa Aesar, 99.0%) were used as received. IR spectra were recorded on a Magna 750 Fourier transform infrared (FT-IR) spectrometer as KBr pellets in the range of 4000−400 cm^{-1}. Microprobe elemental analyses were performed on a field emission scanning electron microscope (FESEM, JSM6700F) equipped with an energy dispersive X-ray spectroscope (EDS, Oxford INCA). X-ray powder diffraction (XRD) patterns were collected on a XPERT-MPD $\theta-2\theta$ diffractometer using graphite-monochromated Cu Kα radiation in the angular range 2θ = 5−85° with a step size of 0.05°. Optical diffuse reflectance spectra were measured at room temperature with a PE Lambda 900 UV−vis spectrophotometer. $BaSO_4$ plate was used as a standard (100% reflectance). The absorption spectrum was calculated from reflectance spectra using the Kubelka−Munk function: $\alpha/S = (1-R)^2/2R$,[16] where α is the absorption coefficient, S is the scattering coefficient which is practically wavelength independent when the particle size is larger than 5 μm, and R is the reflectance. Thermogravimetric analyses were carried out with a NETZSCH STA 449C unit at a heating rate of 15 °C/min under a nitrogen atmosphere. Differential thermal analysis (DTA) was performed under a nitrogen atmosphere on a NETZSCH DTA404PC. The sample and reference (Al_2O_3) were enclosed in Pt crucibles, heated from room temperature to 810 °C, 825 and 875 °C for $RbGeB_3O_7$, $Rb_2GeB_4O_9$, and $Rb_4Ge_3B_6O_{17}$, respectively, and then cooled to 100 °C at a rate of 10 °C/min. The measurements of the powder frequency doubling effect were carried out by means of the modified method of Kurtz and Perry.[17] A 1064 nm radiation generated by a Q-switched Nd: YAG solid-state laser was used as the fundamental frequency light. The SHG wavelength is 532 nm. The SHG efficiency has been shown to depend strongly on particle size, thus the sample was ground and sieved into several distinct particle size ranges (25−45, 45−53, 53−75, 75−105, 105−150, and 150−210 μm). Samples of KDP were prepared as reference materials in identical fashion to assume the SHG effect.

Syntheses of Three Rubidium Borogermanates. All three compounds were synthesized by high-temperature solid-state reactions of the mixtures of Rb_2CO_3, GeO_2, and H_3BO_3, which were thoroughly ground in agate mortars and then transferred to platinum crucibles. The loaded compositions are as follows: Rb_2CO_3 (0.116 g, 0.5 mmol), GeO_2 (0.105 g, 1 mmol), and H_3BO_3 (0.185 g, 3 mmol) for $RbGeB_3O_7$; Rb_2CO_3 (0.231 g, 1 mmol), GeO_2 (0.105 g, 1 mmol), and H_3BO_3 (0.247 g, 4 mmol) for $Rb_2GeB_4O_9$; and Rb_2CO_3 (0.462 g, 2 mmol), GeO_2 (0.105 g, 1 mmol), and H_3BO_3 (0.124 g, 2 mmol) for $Rb_4Ge_3B_6O_{17}$. Colorless single crystals of the three compounds were initially obtained at different reaction temperatures. For $RbGeB_3O_7$, the mixture was heated at 650 °C for 4 days and then cooled to 350 °C at a cooling rate of 3 °C/h before the furnace was switched off; for $Rb_2GeB_4O_9$, the mixture was heated at 750 °C for 3 days and then cooled to room temperature by switching the furnace off; and for $Rb_4Ge_3B_6O_{17}$, the mixture was heated at 725 °C for 4 days and then cooled to 525 °C at a cooling rate of 1 °C/h before the furnace was switched off. The atomic ratios of Rb:Ge determined by energy dispersive spectrometry (EDS) on several single crystals of each compound are 1.1:1.0, 2.1:1.0, and 1.2:1.0 for $RbGeB_3O_7$, $Rb_2GeB_4O_9$, and $Rb_4Ge_3B_6O_{17}$, respectively, which are in good agreement with those determined from single-crystal X-ray structure studies. After proper structural analyses, pure powder samples of $RbGeB_3O_7$, $Rb_2GeB_4O_9$, and $Rb_4Ge_3B_6O_{17}$ were obtained in a quantitative yield by the solid-state reactions of $Rb_2O_3/GeO_2/H_3BO_3$ mixtures in a molar ratio of 1:2:6, 1:1:4, and 2:3:6 at 650 °C for 6 days for $RbGeB_3O_7$, $Rb_2GeB_4O_9$, and $Rb_4Ge_3B_6O_{17}$, respectively. For $Rb_4Ge_3B_6O_{17}$, after initial reactions at 650 °C for 6 days, the sample was taken out, reground, and heated again at 680 °C for 15 days before the furnace was switched off. Their purities were confirmed by XRD powder diffraction studies (Figure S1, Supporting Information). IR data (KBr pellet, cm^{-1}): 1454 (s), 1223 (m), 1027 (s), 878 (s), 697 (m), 577 (w), 478 (w), and 442 (w) for $RbGeB_3O_7$; 1358 (s), 1028 (s), 938 (m), 825 (m), 697 (w), 577 (w), 516 (w), and 442 (w) for $Rb_2GeB_4O_9$; and 1375 (s), 1296 (m), 1033 (s), 950 (w), 863 (w), 767 (s), 598 (w), and 493 (w) for $Rb_4Ge_3B_6O_{17}$ (Figure S2, Supporting Information).

Single-Crystal Structure Determination. Data collections for the above all three compounds were performed on a Rigaku Mercury70 diffractometer equipped with a graphite-monochromated Mo Kα radiation (λ = 0.71073 Å) at 293(2) K. The data sets were corrected for Lorentz and polarization factors as well as for absorption by Multiscan method.[18a] The three structures were solved by the direct methods and refined by full-matrix least-squares fitting on F^2 by SHELX-97.[18b] All of the nonhydrogen atoms were refined with anisotropic thermal parameters except O(5) and O(14) in $Rb_2GeB_4O_9$, which were refined isotropically. The Flack factor of 0.282(9) for $Rb_4Ge_3B_6O_{17}$ indicates the existence of the small extent of the racemic twinning

(13) Kong, F.; Jiang, H. L.; Hu, T.; Mao, J. G. *Inorg. Chem.* **2008**, *47*, 10611.
(14) (a) Parise, J. B.; Gier, T. E. *Chem. Mater.* **1992**, *4*, 1065. (b) Ihara, M. *Yogyo Kyokaishi* **1971**, *79*, 152.
(15) (a) Xiong, D. B.; Zhao, J. T.; Chen, H. H.; Yang, X. X. *Chem.—Eur. J.* **2007**, *13*, 9862. (b) Xiong, D. B.; Chen, H. H.; Li, M. R.; Yang, X. X.; Zhao, J. T. *Inorg. Chem.* **2006**, *45*, 9301.
(16) Wendlandt, W. M.; Hecht, H. G. *Reflectance Spectroscopy*; Interscience: New York, 1966.
(17) Kurtz, S. W.; Perry, T. T. *J. Appl. Phys.* **1968**, *39*, 3798.
(18) (a) *CrystalClear*, version 1.3.5; Rigaku Corp.: Woodlands, TX, 1999. (b) Sheldrick, G. M. *SHELXTL, Crystallographic Software Package*, version 5.1; Bruker-AXS: Madison, WI, 1998.

Table 1. Crystal Data and Structure Refinements for $RbGeB_3O_7$, $Rb_2GeB_4O_9$, and $Rb_4Ge_3B_6O_{17}$

formula	$RbGeB_3O_7$	$Rb_2GeB_4O_9$	$Rb_4Ge_3B_6O_{17}$
fw	302.51	430.77	896.51
space group	$Pna2_1$	$P2_1$	Cc
a (Å)	9.352(5)	6.611(4)	11.845(4)
b (Å)	9.457(5)	9.950(5)	6.968(2)
c (Å)	6.962(4)	13.216(7)	20.253(7)
α (°)	90	90	90
β (°)	90	90.380(7)	103.723(5)
γ (°)	90	90	90
V (Å^3)	615.8(6)	869.3(8)	1624.0(9)
Z	4	4	4
D_c (g·cm^{-3})	3.264	3.291	3.667
μ(Mo Kα) (mm^{-1})	12.816	14.678	17.521
GOF on F^2	1.055	1.006	1.041
Flack factor	0.01(1)	0.04(2)	0.282(9)
$R1$,$wR2$ [$I > 2\sigma(I)$][a]	0.0265, 0.0504	0.0537, 0.0992	0.0152, 0.0354
$R1$, $wR2$ (all data)[a]	0.0294, 0.0518	0.0677, 0.1054	0.0156, 0.0355

[a] $R1 = \sum||F_o| - |F_c||/\sum|F_o|$, and $wR2 = \{\sum w[(F_o)^2 - (F_c)^2]^2/\sum w[(F_o)^2]^2\}^{1/2}$.

for its single crystal. The Flack factors for the other two compounds are close to zero (0.01(1) and 0.04(2), respectively, for $RbGeB_3O_7$, $Rb_2GeB_4O_9$), which indicates that their absolute structures are correct. Crystallographic data and structural refinements for the three compounds are summarized in Table 1. Important bond distances are listed in Table 2. More details on the crystallographic studies as well as atomic displacement parameters are given as Supporting Information.

Computational Descriptions. Single-crystal structural data of the three compounds were used for their electronic and optical property calculations. Band structures and density of states (DOS) were performed with the total-energy code CASTEP.[19] The total energy is calculated with density functional theory (DFT) using Perdew−Burke−Ernzerh of generalized gradient approximation.[20] The interactions between the ionic cores and the electrons are described by the norm-conserving pseudopotential.[21] The following orbital electrons are treated as valence electrons: Rb-4s^{2}4p^{6}5s^1, Ge-4s^{2}4p^2, B-2s^{2}2p^1, and O-2s^{2}2p^4. The number of plane waves included in the basis is determined by a cutoff energy of 500 eV, and the numerical integration of the Brillouin zone is performed using a $3 \times 3 \times 4$, $4 \times 3 \times 2$, and $2 \times 4 \times 1$ Monkhorst−Pack k-point sampling for $RbGeB_3O_7$, $Rb_2GeB_4O_9$, and $Rb_4Ge_3B_6O_{17}$, respectively. The other calculating parameters and convergent criteria were the default values of CASTEP code.

The calculations of linear optical properties in terms of the complex dielectric function $\varepsilon(\omega) = \varepsilon_1(\omega) + i\varepsilon_2(\omega)$ were made. The imaginary part of the dielectric function ε_2 was given in the following equation:[22]

$$\varepsilon_2^{ij}(\omega) = \frac{8\pi^2\hbar^2e^2}{m^2V}\sum_k\sum_{cv}(f_c - f_v)\frac{p_{cv}^i(k)p_{vc}^j(k)}{E_{vc}^2}\delta[E_c(k) - E_v(k) - \hbar\omega] \quad (1)$$

The f_i and f_v represent the Fermi distribution functions of the conduction and valence bands, respectively. The term $P_{cv}^i(k)$ denotes the momentum matrix element transition from the energy level c of the conduction band to the level v of the valence band at a certain k-point in the Brillouin zones, and V is the volume of the unit cell. The m, e, and $\hbar$ are the electron mass, charge, and Plank's constant, respectively.

The second-order optical properties were calculated based on momentum gauge formalism with the minimal-coupling interaction Hamiltonian and within the independent particle approximation.[23,24] The imaginary part of the frequency-dependent second-order susceptibility $\chi^{(2)}(2\omega,\omega,\omega)$ is obtained from the electronic band structures by using the expressions already given elsewhere.[25−28] Then use the Kramers−Kronig

Table 2. Selected Bond Lengths (Å) for $RbGeB_3O_7$, $Rb_2GeB_4O_9$, and $Rb_4Ge_3B_6O_{17}$

	$RbGeB_3O_7$		
Ge(1)−O(7)	1.721(3)	Ge(1)−O(6)	1.731(3)
Ge(1)−O(5)	1.755(3)	Ge(1)−O(4)	1.758(3)
B(1)−O(7)	1.451(6)	B(1)−O(6)	1.476(6)
B(1)−O(1)	1.487(6)	B(1)−O(3)	1.489(6)
B(2)−O(3)	1.340(7)	B(2)−O(4)	1.368(7)
B(2)−O(2)	1.398(7)	B(3)−O(1)	1.331(6)
B(3)−O(5)	1.369(6)	B(3)−O(2)	1.385(6)
	$Rb_2GeB_4O_9$		
Ge(1)−O(7)	1.727(6)	Ge(1)−O(5)	1.735(6)
Ge(1)−O(8)	1.742(6)	Ge(1)−O(2)	1.756(7)
Ge(2)−O(3)	1.730(6)	Ge(2)−O(4)	1.746(6)
Ge(2)−O(1)	1.747(7)	Ge(2)−O(6)	1.757(7)
B(1)−O(8)	1.43(1)	B(1)−O(9)	1.44(1)
B(1)−O(17)	1.50(1)	B(1)−O(14)	1.50(1)
B(2)−O(10)	1.40(1)	B(2)−O(3)	1.48(1)
B(2)−O(13)	1.48(1)	B(2)−O(11)	1.50(1)
B(3)−O(5)	1.45(1)	B(3)−O(9)	1.45(1)
B(3)−O(18)	1.50(1)	B(3)−O(15)	1.51(1)
B(4)−O(7)	1.44(1)	B(4)−O(10)	1.46(1)
B(4)−O(16)	1.50(1)	B(4)−O(12)	1.51(1)
B(5)−O(11)	1.34(1)	B(5)−O(16)	1.36(1)
B(5)−O(6)	1.38(1)	B(6)−O(18)	1.34(1)
B(6)−O(2)	1.35(1)	B(6)−O(17)	1.38(1)
B(7)−O(12)	1.35(1)	B(7)−O(13)	1.36(1)
B(7)−O(4)	1.41(1)	B(8)−O(14)	1.37(1)
B(8)−O(15)	1.38(1)	B(8)−O(1)	1.38(1)
	$Rb_4Ge_3B_6O_{17}$		
Ge(1)−O(15)	1.688(3)	Ge(1)−O(16)	1.728(3)
Ge(1)−O(17)	1.705(3)	Ge(1)−O(8)	1.846(3)
Ge(2)−O(7)	1.670(3)	Ge(2)−O(8)	1.697(3)
Ge(2)−O(2)	1.730(3)	Ge(2)−O(3)	1.847(3)
Ge(3)−O(4)	1.678(3)	Ge(3)−O(5)	1.716(3)
Ge(3)−O(6)	1.771(3)	Ge(3)−O(1)	1.855(4)
B(1)−O(9)	1.391(6)	B(1)−O(7)	1.460(6)
B(1)−O(14)	1.512(6)	B(1)−O(6)	1.560(6)
B(2)−O(2)	1.407(6)	B(2)−O(9)	1.451(6)
B(2)−O(13)	1.519(6)	B(2)−O(5)	1.555(6)
B(3)−O(16)	1.416(6)	B(3)−O(4)	1.486(7)
B(3)−O(12)	1.509(6)	B(3)−O(10)	1.518(6)
B(4)−O(10)	1.419(7)	B(4)−O(1)	1.434(7)
B(4)−O(11)	1.509(6)	B(4)−O(17)	1.555(6)
B(5)−O(14)	1.348(6)	B(5)−O(13)	1.359(6)
B(5)−O(3)	1.370(7)	B(6)−O(12)	1.347(6)
B(6)−O(11)	1.388(6)	B(6)−O(15)	1.400(6)

(19) (a) Segall, M. D.; Lindan, P. J. D.; Probert, M. J.; Pickard, C. J.; Hasnip, P. J.; Clark, S. J.; Payne, M. C. *J. Phys.: Condens. Matter* **2002**, *14*, 2717. (b) Milman, V.; Winkler, B.; White, J. A.; Pickard, C. J.; Payne, M. C.; Akhmatskaya, E. V.; Nobes, R. H. *Int. J. Quantum Chem.* **2000**, *77*, 895.

(20) Perdew, J. P.; Burke, K.; Ernzerhof, M. *Phys. Rev. Lett.* **1996**, *77*, 3865.

(21) Lin, J. S.; Qteish, A.; Payne, M. C.; Heine, V. *Phys. Rev. B: Condens. Matter Mater. Phys.* **1993**, *47*, 4174.

(22) Bassani, F.; Parravicini, G. P. *Electronic States and Optical Transitions In Solids*; Pergamon Press Ltd.: Oxford, U.K., 1975; 149.

(23) Ghahramani, E.; Moss, D. J.; Sipe, J. E. *Phys. Rev. B: Condens. Matter Mater. Phys.* **1991**, *43*, 8990.

(24) Ghahramani, E.; Moss, D. J.; Sipe, J. E. *Phys. Rev. Lett.* **1990**, *64*, 2815.

(25) Duan, C. G.; Li, J.; Gu, Z. Q.; Wang, D. S. *Phys. Rev. B: Condens. Matter Mater. Phys.* **1999**, *60*, 9435.

(26) Guo, G. Y.; Chu, K. C.; Wang, D. S.; Duan, C. G. *Phys. Rev. B: Condens. Matter Mater. Phys.* **2004**, *69*, 205416.

(27) Guo, G. Y.; Lin, J. C. *Phys. Rev. B: Condens. Matter Mater. Phys.* **2005**, *72*, 075416.

(28) Guo, G. Y.; Lin, J. C. *Phys. Rev. B: Condens. Matter Mater. Phys.* **2008**, *77*, 049901.

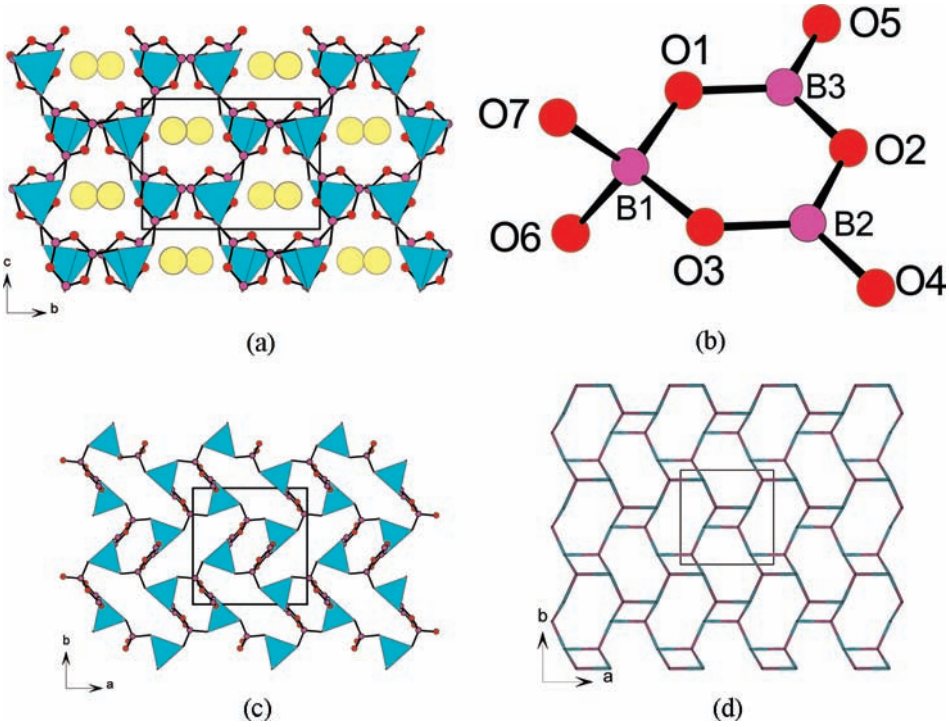

Figure 1. View of the structure of $RbGeB_3O_7$ down the *a*-axis. Rb, Ge, B, and O atoms are drawn as yellow, cyan, pink, and red, respectively (a), a B_3O_7 cluster unit (b), view of the anionic structure of $RbGeB_3O_7$ down the *c*-axis (c), and the topological view of four-connected net of $RbGeB_3O_7$ with the Schläfli symbol $\{4^2.6^3.8\}$ (d).

relations, as required by causality, to obtain the real part

$$\chi'^{(2)}(-2\omega,\omega,\omega) = \frac{2}{\pi}P\int_0^\infty d\omega' \frac{\omega'\chi''^{(2)}(2\omega',\omega',\omega')}{\omega'^2-\omega^2} \quad (2)$$

In the present study, the δ function in the expressions for $\chi^{(2)}(2\omega,\omega,\omega)$[25−27] is approximated by a Gaussian function with $\Gamma = 0.2$ eV. Furthermore, to ensure that the real part calculated via Kramer−Kronig transformation (eq 2) is reliable, at least 300 empty bands were used in SHG calculation. In addition, because DFT-generalized gradient approximation (DFT-GGA) fails to correctly predict the CB energies, the CB energy should be corrected by adding a scissor operator; meanwhile, the momentum matrix elements were also renormalized.[25]

Results and Discussion

Explorations of new second-order NLO materials in the Rb−Ge−B−O system led to three new alkali metal borogermanates, namely, $RbGeB_3O_7$, $Rb_2GeB_4O_9$, and $Rb_4Ge_3B_6O_{17}$. They represent the first compounds in the Rb−Ge−B−O system. It is interesting to note that the pure power samples of $RbGeB_3O_7$ and $Rb_2GeB_4O_9$ were synthesized under the same reaction temperature with different molar ratios of reactants. Hence the Rb/Ge/B molar ratios used have a dramatic effect on the chemical compositions and structures of the compounds formed. The structures of $RbGeB_3O_7$, $Rb_2GeB_4O_9$, and $Rb_4Ge_3B_6O_{17}$ feature three types of anionic open frameworks based on three types of polymeric borate clusters (B_3O_7, B_4O_9, and B_3O_8) interconnected by GeO_4 (and Ge_2O_7) units.

Structure Descriptions. $RbGeB_3O_7$ crystallizes in orthorhombic space group $Pna2_1$ (no. 33); it is isostructural with $CsGeB_3O_7$.[13] Its structure features a 3D network composed cyclic $B_3O_7^{5-}$ anions bridged by Ge(IV) cations with the 1D tunnels along the *a*-axis which is occupied by the Rb^+ cations (Figure 1a). The asymmetric unit of $RbGeB_3O_7$ contains one Rb, one Ge, and three unique B atoms. Ge(1) is tetrahedrally coordinated by four oxygen atoms with Ge−O distances ranging from 1.721(3)−1.758(3) Å, and the O−Ge−O bond angles fall in 105.48(2)−113.69(2)°. Boron(III) atoms show both three-($B(2)O_3$ and $B(2)O_3$) and tetra-coordinated ($B(1)O_4$). The B−O bond distances of the three-coordinated boron atoms, B(2) and B(3), are significantly shorter [1.331(6)−1.398(7) Å] than that of the tetrahedrally coordinated boron atoms [B(1), 1.451(6)−1.489(6) Å]. The O−B−O angles are in the range of 106.2(4)−111.1(4)° for the $B(1)O_4$ tetrahedron and in the range of 113.1(5)−125.3(5)° for the triangular BO_3 groups. The $B(1)O_4$ tetrahedron and the $B(2)O_3$ and $B(2)O_3$ groups form a cyclic $B_3O_7^{5-}$ anion via corner sharing (Figure 1b). Each B_3O_7 cluster is connected to four GeO_4 units by four shared u_2-O atoms, and each GeO_4 tetrahedron also connected to four B_3O_7 clusters. There is no Ge−O−Ge connection in the structure. The B−O−B bond angles of 118.0(4)−124.2(4)° and the B−O−Ge angles of 118.3(3)−135.6(3)° are comparable to those reported in other borogermantes.[6−15] Each Rb^+ cation is nine coordinated by nine oxygen atoms with Rb−O distances in the range of 2.854(3)−3.358(3) Å. Bond valence calculations indicate that the B atoms are in an oxidation state of +3 and the Ge atom is +4, and the calculated total bond valences for B(1)−B(3) and Ge(1) are 3.02, 3.03, 3.08, and 4.08, respectively.[29]

The interconnection of cyclic $B_3O_7^{5-}$ anions bridged by tetrahedrally coordinated Ge(IV) lead to a 3D anionic network with two types of 1D helical tunnels along the *c*-axis (Figure 1c). The large tunnels are based on

(29) (a) Brown, I. D.; Altermatt, D. *Acta Crystallogr.* **1985**, *B41*, 244.

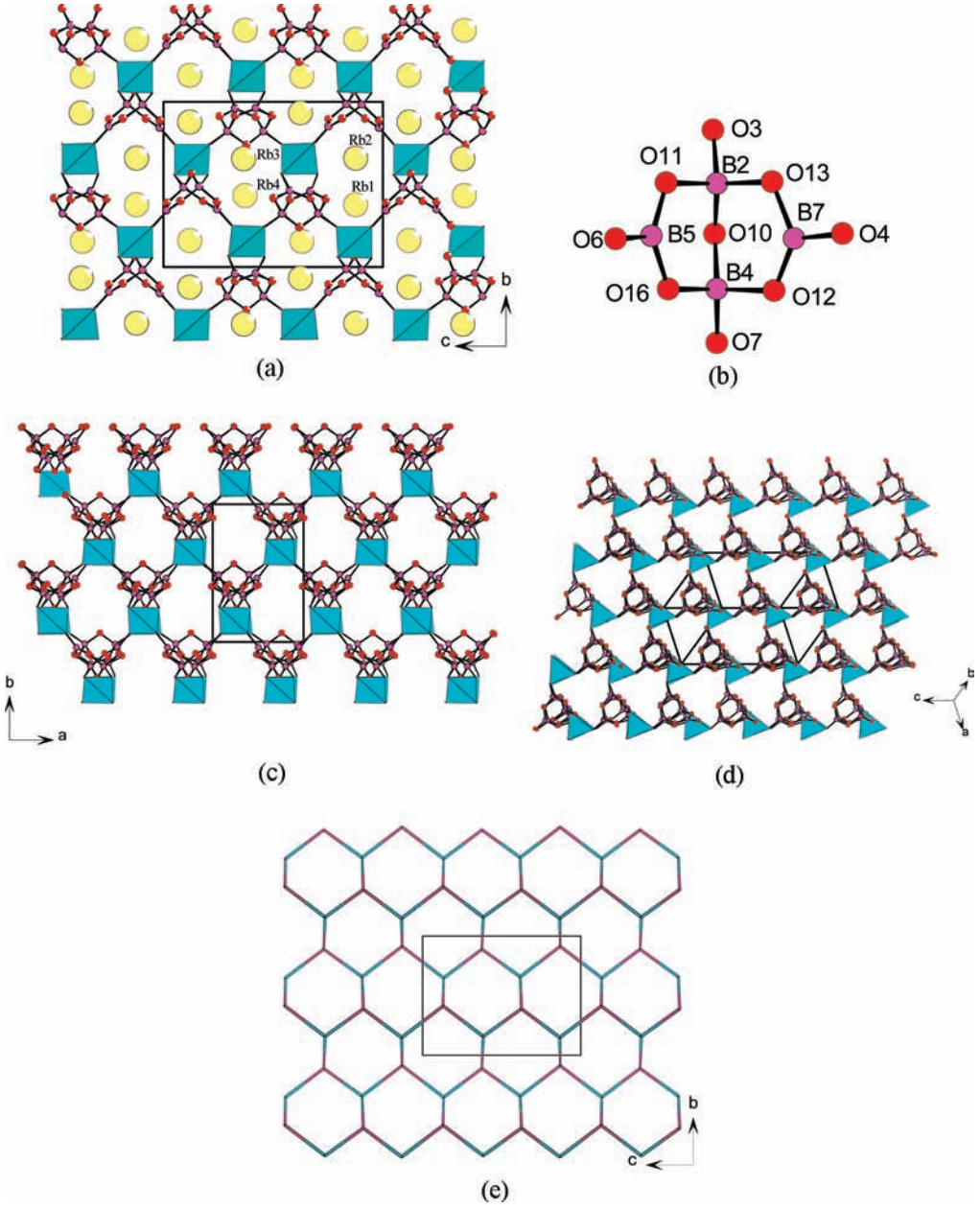

Figure 2. View of the structure of $Rb_2GeB_4O_9$ down the *a*-axis. Rb, Ge, B, and O atoms are drawn as yellow, cyan, pink, and red, respectively (a), a B_4O_9 cluster unit (b), view of the anionic structure of $Rb_2GeB_4O_9$ with 1D 9-/10-MRs tunnels down the *c*-axis (c), view of the anionic structure of $Rb_2GeB_4O_9$ with 1D 9-/10-MRs tunnels down the [112] direction (d), and a topological view of 4-connected net of $Rb_2GeB_4O_9$ with the Schläfli symbol $\{6^6\}$ (e).

10-member rings (MRs) composed on four GeO_4, four BO_4, and two BO_3 groups, whereas the small tunnels are composed of 6-MRs composed of two GeO_4, two BO_4, and two BO_3 units. Each small tunnel is surrounded by four large tunnels, whereas each large tunnel has four large and four small tunnels as its neighbors. Each tunnel can also be described as two interweaving helical tunnels with opposite chirality.

As described above, each B_3O_7 cluster is connected to four GeO_4 units via four shared u_2-O atoms, whereas each GeO_4 tetrahedron is also connected to four B_3O_7 clusters. In the view of the topology, both the Ge(IV) and B_3O_7 clusters act as four-connected nodes. Hence the anionic structure of $RbGeB_3O_7$ can also be described as a four-connected net $SrAl_2$ (sra) with the Schläfli symbol of $\{4^2.6^3.8\}$ (Figure 1d).[30]

$Rb_2GeB_4O_9$ crystallizes in the polar space group $P2_1$ (no. 4), and its structure features a 3D anionic $[GeB_4O_9]^{2-}$ network with strict alternation of B_4O_9 clusters and GeO_4 tetrahedra, forming 1D 9- and 10-MRs tunnels along the *a*-axis. The charge of $[GeB_4O_9]^{2-}$ framework is balanced by Rb^+ ions, which are located in both 9- and 10-MRs tunnels (Figure 2a). The asymmetric unit of $Rb_2GeB_4O_9$ contains four Rb, two Ge and eight B atoms. Both germanium(IV) atoms are tetrahedrally coordinated by four oxygen atoms with Ge−O distances ranging from 1.727(6)−1.757(7) Å, and the O−Ge−O bond angles fall in 102.2(3)−118.6(3)°. Boron(III) atoms show both three- and tetra-coordinated. The B−O bond distances of the three-coordinated boron atoms B(5)−B(8) are significantly

(30) Brese, N. E.; O'Keeffe, M. *Acta Crystallogr.* **1991**, *B47*, 192.

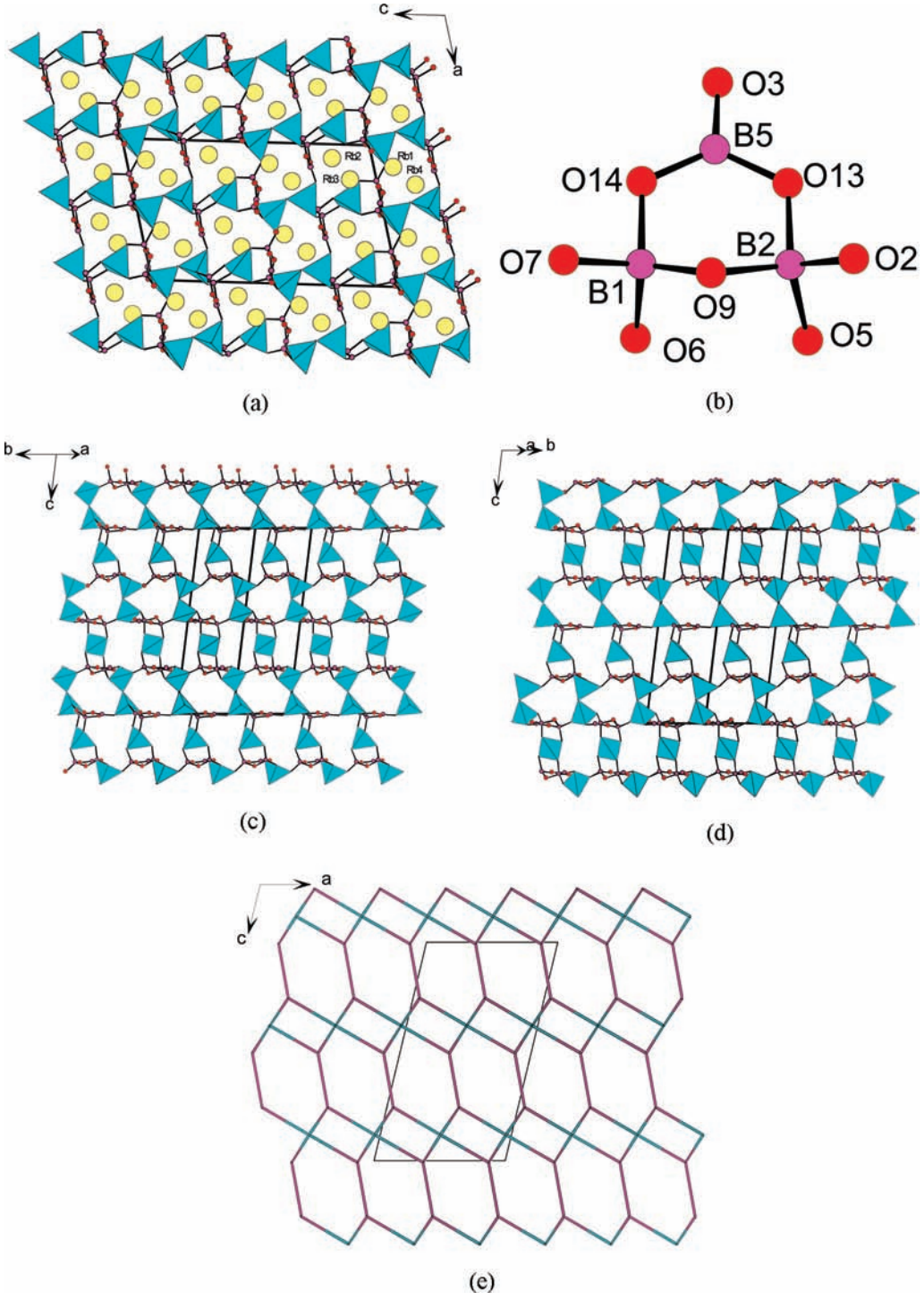

Figure 3. View of the structure of $Rb_4Ge_3B_6O_{17}$ down the *b*-axis. Rb, Ge, B, and O atoms are drawn as yellow, cyan, pink, and red, respectively (a), a B_3O_8 cluster unit (b), view of the anionic structure with 1D 8- and 9-MRs tunnels along the [110] direction (c), the anionic structure with 1D 8- and 9-MRs tunnels along the [−110] direction (d), and a topological view of (4, 6)-connected net of $Rb_4Ge_3B_6O_{17}$ with the Schläfli symbol $\{4^3.6^3\}_2\{4^6.6^6.8^3\}$ (e).

shorter [1.35(1)−1.41(1) Å] than that of the tetrahedrally coordinated ones [B(1)−B(4), 1.40(1)−1.51(1) Å]. The O−B−O angles are in the range of 114.2(9)−125(1) Å for the triangular BO_3 groups and 105.6(4)−114.9(9) Å for the BO_4 tetrahedra. The B_4O_9 cyclic unit is formed by two triangular BO_3 and two BO_4 tetrahedral groups which are connected alternately through corner sharing, and two BO_4 groups are further linked by an u_2-O atom. It contains two approximately perpendicular three-MRs of polyhedra (Figure 2b). Each B_4O_9 cluster is connected to 12 others through four bridging GeO_4 tetrahedra. Similarly, each GeO_4 tetrahedron is also connected to 12 other GeO_4 tetrahedra through four bridging B_4O_9 units. There is no Ge−O−Ge connection in the structure. The B−O−B and B−O−Ge angles are in the range of 112.0(8)−120.0(8)° and 119.6(6)−124.6(6)°, respectively. All those bond distances are comparable to the reported in other borogermantes.[6−15] Rb(1) and Rb(2) are

9-coordinated and Rb(3) is 10-coordinated, whereas Rb(4) is 8-coordinated. The Rb−O distances are in the ranges of 2.775(7)−3.474(7). Bond valence calculations indicate that the B atoms are in an oxidation state of +3 and the Ge atom is +4, the calculated total bond valences for B(1)−B(8) and Ge(1) and Ge(2) are 3.11, 3.11, 3.01, 3.00, 3.09, 3.14, 2.99, 2.96, 4.09, and 4.03, respectively.[29]

The alternate connectivity between B_4O_9 clusters and GeO_4 tetrahedra through their vertices gives rise to the 3D anionic $[GeB_4O_9]_n^{2n-}$ framework with two types of 1D tunnels (Ge_3B_6 9-MRs and Ge_3B_7 10-MRs) along *a*-axis (Figure 2a). Ge_3O_7 10-MRs tunnel consists of three GeO_4, three BO_4, and four BO_3 units and is occupied by Rb(1) and Rb(2). Ge_3O_6 9-MRs tunnel is composed by three GeO_4, four BO_4, and two BO_3 groups with Rb(3) and Rb(4) located in it. Each 9-MRs tunnel is surrounded by four 10-MRs and two other 9-MRs tunnels as its neighbors, whereas each 10-MRs tunnel is surrounded by four 9-MRs and two other 10-MRs tunnels (Figure 2a). $Rb_2GeB_4O_9$ also exhibits 1D 9-/10-MRs tunnels down the *c*-axis and the [112] direction (Figure 2c and d), and there are some obvious differences between them. Along the *c*-axis, it shows an unclosed helical tunnel with an alternate connect of 9- and 10-MRs in ABAB mode. Whereas the tunnel in the [112] direction consists of closed rings of 9- and 10-MRs stacking in AABB mode. As described above, each B_4O_9 cluster is connected to four GeO_4 units and each GeO_4 also connected to four B_4O_9 clusters. From a topological viewpoint, both Ge(IV) and the B_4O_9 clusters act as four connected nodes. The anionic structure of $Rb_2GeB_4O_9$ can also be described as a 3D four connected net diamond (dia) with the Schläfli symbol of $\{6^6\}$ (Figure 2e).[30]

It is interesting to compare the structure of $Rb_2GeB_4O_9$ with those of $K_2GeB_4O_9 \cdot 2H_2O$(*Cc*),[12b] $(CH_3NH_3)_2[GeB_4O_9]$(*C*2),[7d] and $(H_2en)[GeB_4O_9]$($P2_1/n$).[7a] The acentric compounds adopt a similar diamond topology. However, there are still some obvious differences, such as space groups, tunnel orientations, and cations (templates). In $(H_2en)[GeB_4O_9]$, each GeO_4 (or B_4O_9) is linked to 11 others by four bridging B_4O_9 (or GeO_4) units. Such linkage modes gave a different topological symbol of CrB_4 (crb). In addition, $(H_2en)[GeB_4O_9]$ has a larger elliptical channel of 12-MRs.[7c]

$Rb_4Ge_3B_6O_{17}$ crystallizes in the noncentrosymmetric space group *Cc* (no. 9). It forms a new structure type. The structure features a 3D anionic $[Ge_3B_6O_{17}]^{4-}$ network composed 2D layers of corner-sharing B_3O_8 units and Ge_2O_7 dimers that are further bridged by Ge atoms, resulting 8- and 9-MRs tunnels along the *b*-axis that are occupied by the Rb^+ cations (Figure 3a). The asymmetric unit of $Rb_4Ge_3B_6O_{17}$ contains four Rb, three Ge, and six B atoms. All three germanium(IV) atoms are tetrahedrally coordinated by four oxygen atoms with Ge−O distances ranging from 1.670(3)−1.855(4) Å. The O−Ge−O bond angles fall in 101.4(2)−118.7(2)°. Boron(III) atoms show both three- and tetra-coordinated. The B−O bond distances of the three-coordinated boron atoms, B(5) and B(6), are significantly shorter [1.347(6)−1.400(6) Å] than that of the tetrahedrally coordinated boron atoms [B(1)−B(4), 1.391(6)−1.560(6) Å]. The O−B−O angles are in the range of 115.7(4)−125.1(5) Å for the triangular BO_3 groups and 101.2(4)−117.0(4) Å for the BO_4 tetrahedra. The cyclic B_3O_8 cluster is formed by one triangular BO_3 and two BO_4 tetrahedra interconnected via corner sharing (Figure 3b), whereas the Ge_2O_7 dimer is the corner sharing of two GeO_4 terhedra with the Ge(1)−O−Ge(2) bond angle of 127.9(2)°. The B−O−B (115.3(4)−119.7(4) °) and B−O−Ge (110.5(3)−128.6(3) °) angles are comparable to those reported in other borogermantes.[6−15]

The cyclic B_3O_8 clusters are connected with Ge_2O_7 dimers via corner sharing into a 2D double layer parallel to the *ab* plane, forming 1D Ge_4B_4 8-MRs helical tunnels along the *b*-axis which are occupied by Rb(1) and Rb(4) atoms (Figure 3a). Such a type of $[Ge_2B_6O_{17}]^{8-}$ layer has not been reported yet. Neighboring double layers are further bridged by GeO_4 tetrahedra via corner sharing into a novel 3D network with another type of Ge_4B_5 9-MRs helical tunnels along the *b*-axis. Rb(2) and Rb(3) atoms are located at the 9-MRs tunnels (Figure 3a). $Rb_4Ge_3B_6O_{17}$ also exhibits the similar 1D 8- and 9-MRs tunnels along the [110] and [−110] directions (Figure 3c and d). All four Rb^+ cations are 12 coordinated by 12 oxygen atoms with Rb−O bond distances in the range of 2.860(3)−3.615(6) Å. Bond valence calculations indicated that the B atoms are in an oxidation state of +3, and the oxidation state of the Ge atom is +4. The calculated total bond valences for B(1)−B(6) and Ge(1)−Ge(3) are 3.02, 2.99, 2.98, 3.08, 3.10, 2.95, 4.12, 4.19, and 3.99, respectively.[29]

Each B_3O_8 cluster is connected to three Ge_2O_7 dimers and one isolated Ge(3)O_4. Each Ge_2O_7 dimer connects with six B_3O_8 clusters, whereas each isolated Ge(3)O_4 connects with two B_3O_8 clusters. Thus from a topological viewpoint, the B_3O_8 cluster and Ge_2O_7 act as six- and four-connected nodes, respectively, whereas Ge(3)O_4 tetrahedron is merely a linker. The 3D anionic network of $Rb_4Ge_3B_6O_{17}$ can also be described as a 4,6-connected net fsh with the Schläfli symbol of $\{4^3.6^3\}_2\{4^6.6^6.8^3\}$ (Figure 3e).[30]

Optical Properties. Optical diffuse reflectance spectrum studies indicate that $RbGeB_3O_7$, $Rb_2GeB_4O_9$, and $Rb_4Ge_3B_6O_{17}$ are all insulators with an optical band gap of 5.58, 5.54, and 5.42 eV, respectively (Figure S3, Supporting Information). UV absorption spectra of $RbGeB_3O_7$, $Rb_2GeB_4O_9$, and $Rb_4Ge_3B_6O_{17}$ revealed that they are transparent in the range of 430−2500 nm (Figure S4, Supporting Information). IR studies indicate that they show little absorption in the range of 4000−2000 cm^{-1} (2500−5000 nm). Hence these three materials are transparent in the range of 0.43−5.0 μm. The IR spectra of the three compounds display strong absorption bands at 1225−1454 cm^{-1} of the BO_3 groups. The bands for the BO_4 groups appear at 938−1033 cm^{-1}. The absorption peaks at 825−878 cm^{-1} can be assigned to the asymmetrical stretch of the GeO_4 groups. The absorption bands of the symmetrical stretch of the Ge−O bonds are shown in the region of 516−577 cm^{-1}, and bands from 442 to 475 cm^{-1} correspond to the bending vibrations of the Ge−O bonds. The bending vibrations of BO_3 and BO_4 are also shown in 400−700 cm^{-1}(Figure S2, Supporting Information).[31] These assignments are inconsistent with those previously reported.[7,12,13,15]

(31) Nakamoto, K., *Infrared Spectra of Inorganic and Coordination Compounds*; Wiley: New York, 1970.

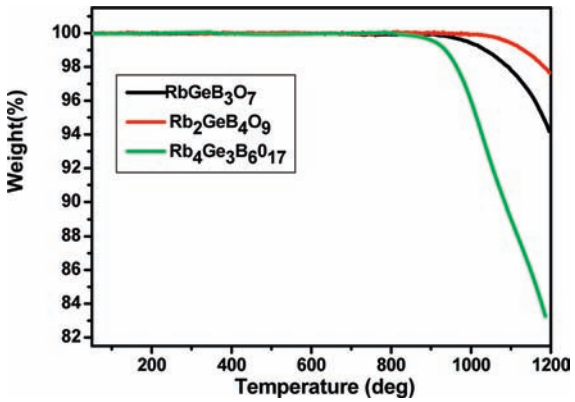

Figure 4. TGA curves for $RbGeB_3O_7$ (black), $Rb_2GeB_4O_9$ (red), and $Rb_4Ge_3B_6O_{17}$ (green).

TGA and DTA Studies. Thermogravimetric analysis (TGA) studies indicate there is no weight loss before 900, 1000, and 850 °C, respectively for $RbGeB_3O_7$, $Rb_2GeB_4O_9$, and $Rb_4Ge_3B_6O_{17}$ (Figure 4). Then they lose weight continuously, corresponding to the evaporation of some versatile components formed by decomposition. The total weight losses at 1200 °C are 5.8% for $RbGeB_3O_7$, 2.4% for $Rb_2GeB_4O_9$, and 16.7% for $Rb_4Ge_3B_6O_{17}$, respectively. Differential thermal analysis (DTA) diagrams of $RbGeB_3O_7$, $Rb_2GeB_4O_9$, and $Rb_4Ge_3B_6O_{17}$ exhibit endothermic peaks at 750, 773, and 790 °C, respectively, in the heating curve, but no exothermic peaks are found in the cooling curves (Figure 5), indicating that all three compounds melt incongruently at around 750, 773, and 790 °C, respectively.[32]

SHG Measurements. $RbGeB_3O_7$, $Rb_2GeB_4O_9$, and $Rb_4Ge_3B_6O_{17}$ all display acentric structures; therefore it is worthy to examine their SHG properties. SHG measurements on a Q-switched Nd:YAG laser with the sieved powder samples (70−100 mesh) revealed that $RbGeB_3O_7$, $Rb_2GeB_4O_9$, and $Rb_4Ge_3B_6O_{17}$ display moderate-strong SHG responses of approximately 1.3, 2.0, and 1.3 × KDP, respectively. Furthermore, all three compounds were found to be type 1 phase matchable (Figure 6). The SHG responses could be mainly attributed to the triangular BO_3 groups in their structures.

Theoretical Studies. The calculated band structures of $RbGeB_3O_7$, $Rb_2GeB_4O_9$, and $Rb_4Ge_3B_6O_{17}$ are plotted in Figure 7, and the state energies of the lowest conduction band (L-CB) and the highest valence band (H-VB) at high symmetry points of the first Brillouin zone are listed in Table S1, Supporting Information. It is clear that $RbGeB_3O_7$ is a direct band gap insulator (from G to G) with a band gap of 4.19 eV. For $Rb_2GeB_4O_9$, the L-CB is at the G point, and the H-VB is at the B point. So it is an indirect band gap crystal, and the band gap is 3.54 eV. $Rb_4Ge_3B_6O_{17}$ is also an indirect band gap crystal with the L-CB at G point and the H-VB at A point, and its band gap is 3.29 eV. The calculated band gaps are smaller than the experimental ones (5.58 eV for $RbGeB_3O_7$, 5.54 eV for $Rb_2GeB_4O_9$, and 5.42 eV for $Rb_4Ge_3B_6O_{17}$). This is not surprising as it is well-known that the GGA does not accurately describe the eigenvalues of the electronic states, which causes quantitative underestimation of band gaps, especially for insulators.[33] Hence during the subsequent optical properties calculations, the scissor values of 1.39, 2.0, and 2.13 eV were applied for $RbGeB_3O_7$, $Rb_2GeB_4O_9$, and $Rb_4Ge_3B_6O_{17}$, respectively.

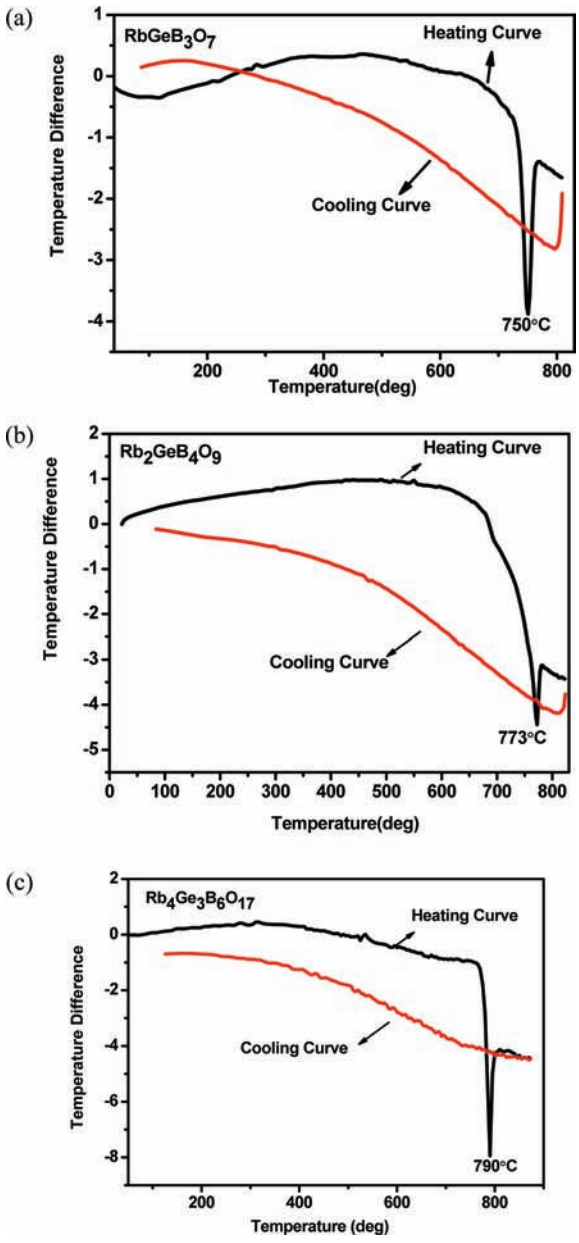

Figure 5. DTA curves for $RbGeB_3O_7$ (a), $Rb_2GeB_4O_9$ (b), and $Rb_4Ge_3B_6O_{17}$ (c).

The bands can be assigned according to the total and partial DOS, as plotted in Figure S5, Supporting Information. It is found that the DOS pictures of the three compounds are very similar; hence we take $RbGeB_3O_7$ as the example to describe them in detail. For $RbGeB_3O_7$, the bottom-most VB region near −23.8 eV comes from Rb-4s states, and the VBs ranging from −20.3 to −15.8 eV

(32) Pan, S. L.; Watkins, B.; Smit, J. P.; Marvel, M. R.; Saratovsky, I.; Poeppelmeier, K. R. *Inorg. Chem.* **2007**, *46*, 3851.

(33) (a) Godby, R. W.; Schluter, M.; Sham, L. J. *Phys. Rev. B: Condens. Matter Mater. Phys.* **1987**, *36*, 6497. (b) Okoye, C. M. I. *J. Phys.: Condens. Matter* **2003**, *15*, 5945. (c) Terki, R.; Bertrand, G.; Aourag, H. *Microelectron. Eng.* **2005**, *81*, 514. (d) Jiang, H. L.; Kong, F.; Mao, J. G. *J. Solid State Chem.* **2007**, *180*, 1764.

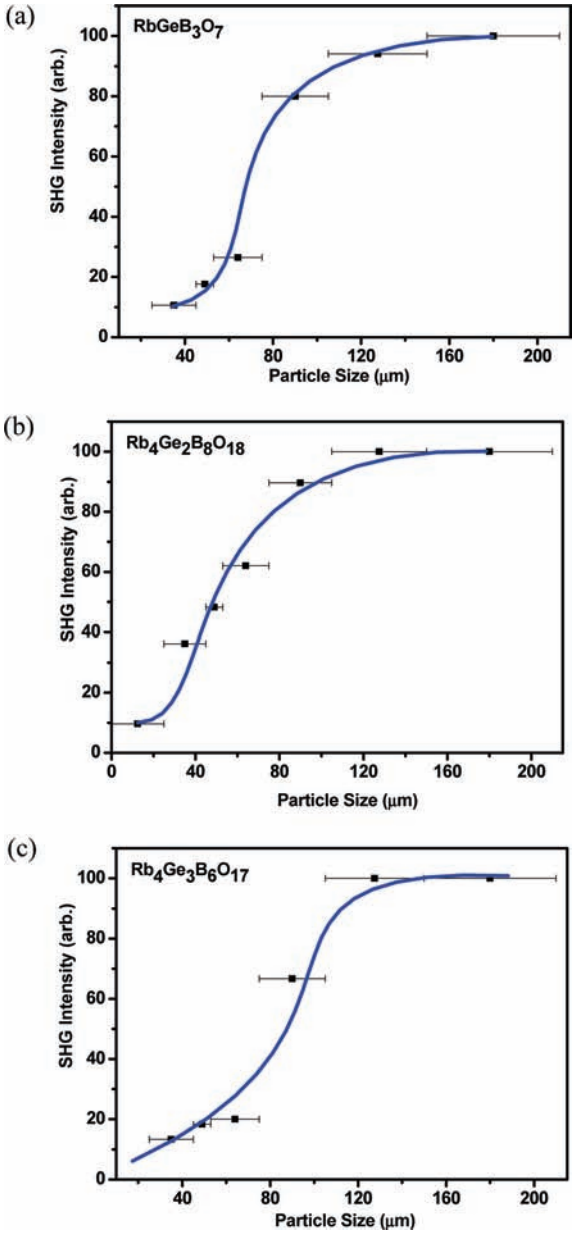

Figure 6. Phase-matching curves for $RbGeB_3O_7$ (a), $Rb_2GeB_4O_9$ (b), and $Rb_4Ge_3B_6O_{17}$ (c). The curve drawn is to guide the eye and not fit to the data.

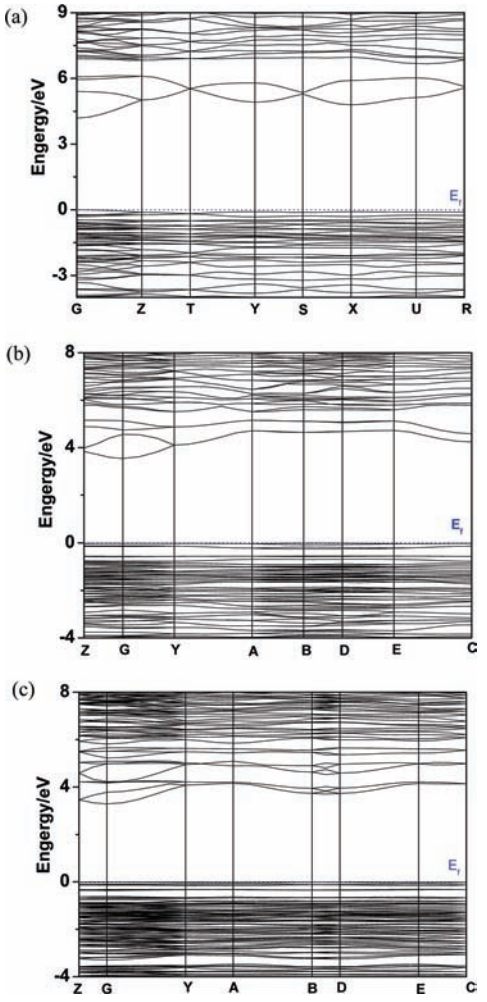

Figure 7. Band structures for $RbGeB_3O_7$ (a), $Rb_2GeB_4O_9$ (b), and $Rb_4Ge_3B_6O_{17}$ (c).

are mainly originated from O-2s, mixing with some B-2s, 2p states. Rb-4p states contribute to the peak near −8.0 eV. In the Fermi level region, namely, −9.3 to 0 eV in VB and 4.2−15 eV in CB, O-2p states overlap with Ge-4p and B-2p, indicating the covalent interactions of B−O and Ge−O bonds.

Population analyses allow for a more quantitative bond analysis (Table S2, Supporting Information). The calculated bond orders of B−O and Ge−O bonds are 0.57−0.91 e and 0.46−0.64 e, respectively (covalent single bond order is generally 1.0 e), so we can say that the B−O bonds are stronger than Ge−O bonds. In addition, the bond orders of B−O bonds in BO_3 groups (0.75−0.91 e) are significantly larger than those in BO_4 groups (0.57−0.76 e).

Furthermore, we also explored the linear and nonlinear optical properties of these polar crystals. It is noticeable that all of the optical properties calculations in this paper were based on their principal dielectric axis coordinate systems. For the determination method of the principal dielectric axes of the monoclinic crystals, please see ref 5b and the rotation angles (θ) between the original coordinate axes and the principal dielectric axes in the *ac* plane were calculated to be −10.833° and −19.975°, respectively, for $Rb_2GeB_4O_9$ and $Rb_4Ge_3B_6O_{17}$.

The linear optical response properties of these compounds were examined through calculating the complex dielectric function $\varepsilon(\omega) = \varepsilon_1(\omega) + i\varepsilon_2(\omega)$. The imaginary part ($\varepsilon_2(\omega)$) can be used to describe the real transitions between the occupied and unoccupied electronic states. The imaginary parts of the frequency-dependent dielectric functions of these compounds show obvious anisotropy along three principal dielectric axis directions (Figure S6, Supporting Information). The curves of the averaged imaginary part and real part of dielectric function were obtained by $\varepsilon^{ave} = (\varepsilon_x + \varepsilon_y + \varepsilon_z)/3$, as displayed in Figure S7, Supporting Information for these compounds. It is found that the strongest adsorption peaks of these compounds are very close to each other, for example, their first peaks are located around 10.0 eV, which can be mainly assigned to the electronic interband transitions from the O-2p to B-2p and Ge-4s, 4p states. The average static dielectric constants $\varepsilon(0)$ are 2.55, 2.46,

and 2.59 for $RbGeB_3O_7$, $Rb_2GeB_4O_9$, and $Rb_4Ge_3B_6O_{17}$, respectively. The dispersion curves of refractive indices calculated by the formula $n^2(\omega) = \varepsilon(\omega)$ indicate that, for $RbGeB_3O_7$, there is an order of $n^z > n^y > n^x$ in the low-energy range (Figure S8, Supporting Information), for $Rb_2GeB_4O_9$, the order is $n^x > n^z > n^y$, but n^x and n^z are much larger than n^y (Figure S8, Supporting Information), and for $Rb_4Ge_3B_6O_{17}$, the order is $n^x > n^y > n^z$ (Figure S8, Supporting Information). The n^x, n^y and n^z values at 1064 nm for $RbGeB_3O_7$ are 1.586, 1.602, and 1.616, respectively, and the corresponding values are 1.583, 1.557, and 1.580 for $Rb_2GeB_4O_9$, and 1.636, 1.616, and 1.590 for $Rb_4Ge_3B_6O_{17}$.

Based on the space groups and the Kleinman symmetry, $RbGeB_3O_7$, $Rb_2GeB_4O_9$, and $Rb_4Ge_3B_6O_{17}$ have three, four, and six nonvanishing independent SHG coefficient tensors, respectively, and the frequency-dependent SHG coefficients of these crystals are plotted in Figure S9, Supporting Information. For $RbGeB_3O_7$, the values of d_{15}, d_{24} and d_{33} at 1064 nm (1.165 eV) are 2.44, 3.39, and 4.05×10^{-9} esu, respectively. For $Rb_2GeB_4O_9$, the values of d_{14}, d_{16}, d_{22}, and d_{34} at 1064 nm are 3.09, 1.19, 0.09, and 1.42×10^{-9} esu, respectively. For $Rb_4Ge_3B_6O_{17}$, the values of d_{11}, d_{12}, d_{13}, d_{24}, d_{31}, and d_{33} at 1064 nm are 2.67, 2.50, 1.52, 1.05, 1.50, and 1.43×10^{-9} esu, respectively. It is clear that the highest SHG coefficients follow the order of $RbGeB_3O_7 > Rb_2GeB_4O_9 > Rb_4Ge_3B_6O_{17}$. It is expected that π-conjugated BO_3 groups have much larger contribution to SHG response than that of BO_4 and GeO_4 groups in their frameworks, and the above order matches well with the total numbers of BO_3 groups per 1000 Å^3 in these three compounds (13 BO_3 per 1000 Å^3 for $RbGeB_3O_7$, 9.2 for $Rb_2GeB_4O_9$, and 5 for $Rb_4Ge_3B_6O_{17}$). It also should be mentioned that the packing fashion of these borate groups and the cations used may also affect the macroscopic polarizations and SHG coefficients. These calculated SHG coefficients are close to our experimental values, which are 1.3, 2.0, and 1.3 × KDP ($d_{36} = 1.1 \times 10^{-9}$ esu) for $RbGeB_3O_7$, $Rb_2GeB_4O_9$, and $Rb_4Ge_3B_6O_{17}$, respectively.

Conclusions

In summary, three novel rubidium borogermanates with noncentrosymmetric structures $RbGeB_3O_7$, $Rb_2GeB_4O_9$, and $Rb_4Ge_3B_6O_{17}$ have been synthesized by high-temperature solid-state reactions. They adopt three types of 3D anionic open frameworks based on polymeric borate clusters and GeO_4 (and Ge_2O_7) groups. $Rb_4Ge_3B_6O_{17}$ is the first borogermanate that contains both isolated "GeO_4" tetrahedron and Ge_2O_7 dimer as linkers between polymeric borate clusters. SHG measurements indicate that they exhibit a response of about 1.3, 2.0, and 1.3 × KDP, respectively. They are also phase matchable and of very high thermal stability. The inclusion of germinate group into the borate system will not only enrich the structure chemistry of metal borates but also afford new SHG materials with improved physical properties. Our future research efforts will be devoted to the preparations of other boron-rich borogermanates with enhanced SHG properties by the inclusion of lone pair containing Pb^{2+} and Bi^{3+} cations or transition-metal ions with d^0 electronic configurations, such as Ti^{4+}, V^{5+}, and Mo^{6+}, etc. These two types of cations normally exhibit asymmetric coordination geometries due to the second-order Jahn−Teller distortion.

Acknowledgment. This work was supported by the National Natural Science Foundation of China (nos. 20731006, 20825104, 20821061, and 21001107) and the Key Project of FJIRSM (no. SZD07001-2).

Supporting Information Available: Calculated bond orders, simulated and experimental XRD powder patterns, IR spectra, UV spectra and optical diffuse reflectance, and DOS and partial DOS diagrams as well as figures of theoretical calculations. This material is available free of charge via the Internet at http://pubs.acs.org.